Optical and mass spectrometric investigations of ions and neutral species in SF_6 radio-frequency discharges

R. Foest
Institut für Niedertemperatur-Plasmaphysik, D-17489 Greifswald, Germany

J. K. Olthoff,[1] R. J. Van Brunt,[1] E. C. Benck,[2] and J. R. Roberts[2]
[1]*Electricity Division, Electronics and Electrical Engineering Laboratory, National Institute of Standards and Technology, Gaithersburg, Maryland 20899*
[2]*Atomic Physics Division, Physics Laboratory, National Institute of Standards and Technology, Gaithersburg, Maryland 20899*

(Received 14 February 1996)

Radio-frequency (rf) discharges at 13.56 MHz were generated in pure SF_6 using a capacitively coupled, parallel-plate GEC reference cell for gas pressures in the range of 4–33.3 Pa (30–250 mTorr) and for peak-to-peak applied rf voltages in the range of 100–300 V. The following measurements were made during operation of the discharge: (1) electrical characteristics which included power dissipation, voltage-current phase angle, and the dc self-bias; (2) time-averaged vertical and horizontal profiles of the optical emissions from neutral atomic fluorine for the $2p^43p'\ ^2F^0_{7/2}\rightarrow 2p^43s'\ ^2D_{5/2}$ and $2p^43p\ ^2P^0_{3/2}\rightarrow 2p^43s\ ^2P_{3/2}$ transitions; (3) spatially resolved, laser-induced fluorescence (LIF) utilizing the $2p^43s\ ^4P_{5/2}$ metastable level of atomic fluorine; (4) mass spectra of neutral species in the plasma; and (5) kinetic-energy distributions and relative fluxes of mass-selected positive ions extracted from the plasma through a 0.1 mm diameter orifice in the grounded electrode. The dependence of the electrical characteristics on gas pressure confirms previous observations and model predictions which indicate, for example, that the plasma becomes more resistive as pressure increases. The optical-emission and LIF results are also consistent with previously reported pronounced peaks in emission intensity in front of the powered electrode and a complex double-layer formation at the plasma-sheath boundary, which can be attributed to the strong electron-attaching properties of the gas. From the mass-spectrometric observations of the neutral gas constituents, it can be inferred that a significant fraction (as much as 80% in some cases) of the SF_6 in the cell can be dissociated or decomposed when the discharge is on for an input gas flow rate of 1.5×10^{-6} mol s^{-1} (2.0 cubic centimeters per minute at standard temperature and pressure). The measured ion-energy distributions exhibit deviations from the simple "rf-saddle structure" that become more pronounced with decreasing ion mass. The ion-energy distributions also exhibit pronounced dependences on pressure and applied voltage that appear to be consistent with corresponding changes in the electrical characteristics and LIF. Changes in electrode-surface conditions produced by the discharge were found to dramatically affect the ion-energy distributions, LIF, and electrical characteristics. [S1063-651X(96)05508-0]

PACS number(s): 52.50.Pi, 52.25.Rv, 52.70.Vc

I. INTRODUCTION

In recent years there has been considerable interest in learning more about radio-frequency (rf) discharges in SF_6 and its mixtures with other gases, especially O_2, because of their application in dry etching and other plasma processing of solid materials [1–7]. Results from many observations of rf-discharge behavior in SF_6 have been reported. Among these are (1) measurements of electrical characteristics [7,8], (2) measurements of spatial distributions of time-averaged [9] and time-resolved [10–12] optical emission, (3) measurements of time-averaged and time-resolved electron and ion concentrations [13,14], (4) mass-spectrometric observations of neutral and ionic species [1,2,15,16], and (5) measurements of ion kinetic-energy distributions [1,17]. Radio-frequency discharges in SF_6 have also been the subject of numerous modeling efforts. Simulations based on various computational schemes have been used to predict such properties of the discharge as (1) electron and chemical kinetics and neutral species densities [18], (2) spatiotemporal-dependent ionization rates and ion and electron densities [11,19–23], and (3) optical-emission profiles [11,21–23]. In some cases, it has been possible to derive information from models about the electrical characteristics of the discharge, such as the power dissipation and related voltage-current phase shift [21]. The rates for elementary processes of importance in SF_6 discharges have also been compiled and reviewed [23,24].

From the results of both the model calculations and observations, it has been found that the behavior of rf discharges in electron attaching (electronegative) gases such as SF_6 differs considerably from that of rf discharges in electropositive gases, such as argon, in which electron-attachment to atomic species does not occur. The differences between rf discharges in electropositive and electronegative gases are largely a consequence of the important roles played by negative ions and related electron-attachment and detachment processes in the latter case. It was found from simulations of SF_6 discharges [21] that the majority of charged particles in the bulk of the rf plasma consists of positive and negative ions, with ion densities significantly exceeding electron densities. Despite this difference in densities, electrons

still represent the dominant component of the conduction current due to their relatively high mobility. Time-averaged electric-field strengths in the bulk of the SF_6 plasma are much greater than in the bulk of an Ar plasma [11,19], and consequently there can be significant contributions to the net ionization of SF_6 from electron collisions that occur in the bulk region. The relatively high field in the bulk of the SF_6 discharge results from the tendency of the field to approach a value at which the ionization and electron attachment rates are approximately equal, in accordance with the experimental observations of Ogle and Woolsey [25].

As for the case of discharges in argon, the ionization rate in SF_6 discharges is peaked near the electrodes at the sheath boundary. The optical emission, which in pure SF_6 is dominated by atomic fluorine, is correlated with the ionization rate and also peaks near the electrodes. Other characteristics of SF_6 rf discharges are (1) tendency for the sheath to form a double layer [20,21]; (2) tendency for the sheath region to become very narrow or constricted compared with an electropositive discharge [19,21]; and (3) tendency for the plasma to become increasingly more resistive as pressure increases [7,8,21], which is again in contrast to the capacitive behavior characteristic of rf discharges in electropositive gases. For mixtures of SF_6 with small quantities of N_2, the discharge has been observed to become even slightly inductive under a narrow range of conditions [8].

From mass spectrometric observations [1,15] it has been determined that the predominant positive ion that strikes the electrode surfaces in a SF_6 rf discharge is SF_3^+ followed by SF_5^+. However, many other ions are observed including SF_2^+, SF^+, F^+, S_2F^+, and S^+, and the relative concentrations of these ions depend on such conditions as gas pressure, flow rate, and rf power. The major negative ions observed mass spectrometrically in SF_6 rf discharges are F^-, SF_6^-, and SF_5^- [16]. The presence of F^- in SF_6 rf discharges has also been verified by laser-beam induced photodetachment [14]. The distributions in kinetic energy of ions that bombard the electrode in a SF_6 rf discharge have been measured by the retarding potential difference method [1,17]. The results from these measurements, however, cannot be interpreted easily because the method does not allow the contributions from ions of different mass-to-charge ratio to be distinguished.

In the present work, we report observations of metastable atomic fluorine by laser-induced fluorescence (LIF) and the first reported measurements of the ion-energy distributions (IEDs) for mass-identified positive ions that impact the grounded electrode in 13.56 MHz SF_6 rf discharges. The results from these measurements are correlated with results from measurements of the profiles for optical emission from atomic fluorine, electrical characteristics of the discharge, and mass spectra of neutral species extracted from the plasma under similar or identical conditions. The data obtained in the present work are shown to be consistent with results from previous experimental observations and model calculations. Additionally, the measured ion-energy distributions are found to exhibit peculiar pressure- and voltage-dependent structures that are indicative of the constricted sheath and possibly of the double sheath layer formation that are characteristics of rf discharges in SF_6. Results from the neutral mass spectra are used to estimate the degree of SF_6 dissociation and/or decomposition in the discharge. Significant effects of discharge-induced electrode conditioning on both the LIF and IED measurements are also reported. Preliminary results from this work have previously been presented [28,29].

II. EXPERIMENTS

A. Discharge conditions and electrical measurements

The rf discharges investigated in this work were generated in a "GEC Reference Cell" [26,27] at a frequency of 13.56 MHz. The cell consists of two 102 mm diameter parallel-plate electrodes separated by a distance of 25.4 mm in a stainless-steel chamber. The top electrode and the chamber walls are at the same local ground potential, and the bottom (powered) electrode is capacitively coupled to an external rf power supply and contains small holes in a "showerhead" arrangement through which gas flows into the chamber. For the optical-emission and LIF studies, both electrodes were made of aluminum as specified in the original reference cell design [27]. For the mass-spectrometric and IED measurements, the top grounded electrode was replaced with a stainless-steel electrode that contained a small (0.1 mm diameter) orifice in the center through which ions and neutral species were sampled. The SF_6 gas flow rates were determined by a mass flow controller. For the optical-emission and LIF studies, the flow rate was 7.5×10^{-6} mol/s (10 SCCM) (SCCM denotes cubic centimeter per minute at STP) and for the mass-spectrometric and IED measurements, the flow rate was 1.5×10^{-6} mol/s (2.0 SCCM). The experiments were performed with high purity (99.99%) SF_6.

The electrical characteristics of the discharge were measured by methods that have been documented previously [30,31]. The following electrical parameters were measured (1) the fundamental Fourier component of the voltage at the electrode (V_1), (2) the fundamental Fourier component of the current at the electrode (I_1), (3) the phase angle (ϕ_1) between V_1 and I_1, (4) the power ($\Sigma_{i=1}^{5} V_i I_i \cos\phi_i$), (5) the impedance ($V_1/I_1$), and (6) the dc self-bias (V_b). These parameters were determined simultaneously with the optical and mass spectrometric measurements. Peak-to-peak applied voltages were in the range of 100—300 V and the steady-state SF_6 gas pressures used were in the range of 4–33.3 Pa (30–250 mTorr).

B. Optical-emission spectroscopy and LIF

Figure 1 shows an energy-level diagram indicating the electronic states and transitions for neutral atomic fluorine (F I) that are relevant to the LIF measurements and the optical-emission spectra (OES) that were observed in the present investigations. The LIF measurements involve excitation from the metastable $2p^4 3s\ ^4P_{5/2}$ state to the $2p^4 3p\ ^4S^0_{3/2}$ state in the quartet system using a beam from a pulsed Nd:YAG (YAG denotes yttrium aluminum garnet) pumped dye laser at a wavelength of 623.965 nm. The subsequent emission from the transition $2p^4 3p\ ^4S^0_{3/2} \rightarrow 2p^4 3s\ ^4P_{3/2}$ at 634.851 nm was observed at an angle of 45° with respect to the laser-beam direction.

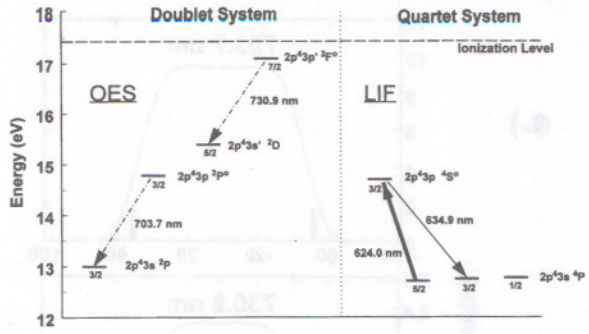

FIG. 1. Fluorine energy levels and corresponding transitions used for the OES and LIF measurements.

Through the use of a beam steering mechanism [32], it was possible to determine the spatial dependence of the LIF signal within the discharge.

The transitions $2p^4 3p'\ ^2F^0_{7/2} \rightarrow 2p^4 3s'\ ^2D_{5/2}$ (730.9 nm) and $2p^4 3p\ ^2P^0_{3/2} \rightarrow 2p^4 3s\ ^2P_{3/2}$ (703.7 nm) in the doublet system were used for the OES observations reported here. The emission corresponding to the $2p^4 3p\ ^4S^0_{3/2} \rightarrow 2p^4 3s\ ^4P_{3/2}$ transition used in the LIF measurements was also observed, but was not used to determine the spatial profiles reported here. Both the OES and LIF data are "time averaged" in the sense that they represent the net intensities recorded for a large number of rf cycles that are not correlated with any particular phase of the rf cycle. The OES data were obtained using the spectrometer and associated steering and recording systems described in Ref. [32]. Each data point represents the mean of ten consecutive measurements of the average photomultiplier current. In the case of the LIF measurements the photomultiplier signal was integrated for 50 ns after each laser pulse. The low intensity of the LIF signal is due to the fact that Russell-Saunders (LS) coupling does not strictly hold for fluorine and the $2p^4 3s\ ^4P_{5/2}$ state can be radiatively depopulated by a vacuum ultraviolet (vuv) intercombination line to the $2p^5\ ^2P^0_{3/2}$ ground state. Typically the average yield was less than 1.0 photons per laser pulse. The data reported represent the averages of six separate measurements of 10^3 laser pulses per measurement. In order to obtain "one-dimensional" OES horizontal spatial emission profiles that can be compared directly with the LIF results, it was necessary to perform an Abel inversion of the raw intensity data from the OES recordings [32]. All of the OES data presented for the horizontal emission intensity profiles have been Abel inverted.

C. Mass spectrometry and ion-energy analysis

The system used to obtain mass spectra of neutral species and to measure time-averaged kinetic-energy distributions of ions impinging on the grounded electrode is identical to that used previously to investigate rf discharges in other gases such as argon, nitrogen, and oxygen [33,34]. The ions or neutral species are sampled through a 0.1 mm diameter orifice in the center of the grounded electrode. For IED measurements, the ions that pass through the orifice are accelerated and focused into a 45° electrostatic energy selector. After being selected according to their energy, the ions enter a quadrupole rf mass filter where they are also selected according to their mass-to-charge ratio (m/z). The system is operated so that ions always pass through the energy and mass selectors with the same kinetic energy regardless of their initial energy upon entering the sampling orifice. The energy resolution of the selector was fixed at a value of $\Delta\varepsilon = 1.5$ eV, full width at half maximum.

A channeltron electron multiplier with associated pulse counting electronics served as the ion detector of the mass filter. The reported IEDs correspond to fluxes (ion counts per second) recorded for ions incident on the grounded electrode surface with fixed m/z at different energies. At each nominal energy ε the recorded flux corresponds to ions with energies in the range between $\varepsilon - \Delta\varepsilon/2$ and $\varepsilon + \Delta\varepsilon/2$ determined by the energy resolution of the instrument. The ion-flux recording times were the same for all energies. Although the uncertainty in the energy scale is estimated to be ± 1.5 eV, no corrections have been made for possible shifts due to contact potentials or electrode surface charging [34]. As will be discussed later, significant shifts were observed in IEDs that can be attributed to changing conditions of the electrode surface during operation of the discharge.

The mass spectra of neutral species were obtained by ionizing the gas that effused through the orifice in the electrode with a 70.0 ± 1.5 eV electron beam prior to energy and mass selection. The differences in the mass spectra obtained with and without operation of the discharge were used to estimate the degrees of SF_6 dissociation-decomposition in the discharge.

III. RESULTS

A. Optical emission and LIF

Consistent with results reported from a previous investigation [9], it was found that the predominant optical emission from discharges in pure SF_6 is associated with atomic fluorine. The observed F I emission is believed to result primarily from electron-impact excitation, i.e.,

$$e + \mathrm{F} \rightarrow \mathrm{F}^* + e \rightarrow \mathrm{F} + h\nu + e, \tag{1}$$

with minor contributions from the process of dissociative excitation of SF_6 [35,36], e.g.,

$$e + \mathrm{SF_6} \rightarrow \mathrm{SF_5} + \mathrm{F}^* + e$$

$$\mathrm{F}^* \rightarrow \mathrm{F} + h\nu. \tag{2}$$

Here $h\nu$ is the energy of the emitted photon.

The OES results reported here apply specifically to the 703.7 nm and the 730.9 nm lines as noted above (see Fig. 1). Results for the vertical axial-position-dependent emission from atomic fluorine at 703.7 nm and 730.9 nm are shown, respectively, in Figs. 2(a) and 2(b). The axial distance is measured from the powered electrode so that the maximum distance of 25.4 mm corresponds to the position of the grounded electrode. Figure 2(c) shows the corresponding axial position dependence of the intensity ratio [I(730.9 nm)/I(703.7 nm)] for these lines.

In Fig. 3 is shown the corresponding vertical axial distance dependence of the LIF signal for the same discharge

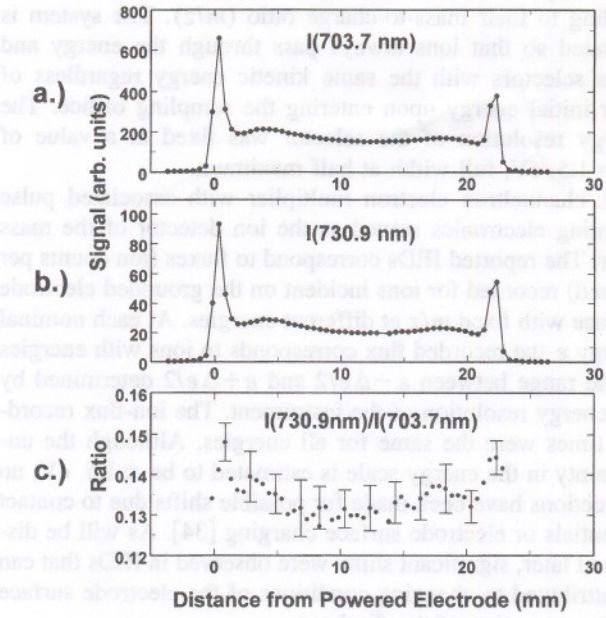

FIG. 2. Axial dependence of the OES intensities for (a) the 703.7 nm emission, (b) the 730.9 nm emission, and (c) the ratios of the 730.9 nm to 703.7 nm emissions. The data were obtained at a gas pressure of 33.3 Pa and peak-to-peak applied voltage of 300 V.

conditions. The results displayed in Figs. 2 and 3 were obtained for a gas pressure of 33.3 Pa and a peak-to-peak applied voltage of 300 V.

For the discharge conditions that were used, both the OES and LIF data show sharp peaks in the time-averaged emission intensity close to the electrode surfaces indicative of a narrow sheath region and consistent with earlier experimental results and predictions [9–12,21,22]. The results from both observations also exhibit secondary maxima in intensity between the main peaks and the lower, more uniform emission intensity from the bulk. These secondary maxima that appear near both electrodes are indicative of the previously reported double-layer formation in the sheath associated with rf discharges in SF_6. The emission from the bulk region between the maxima at the two electrodes exhibits a weak

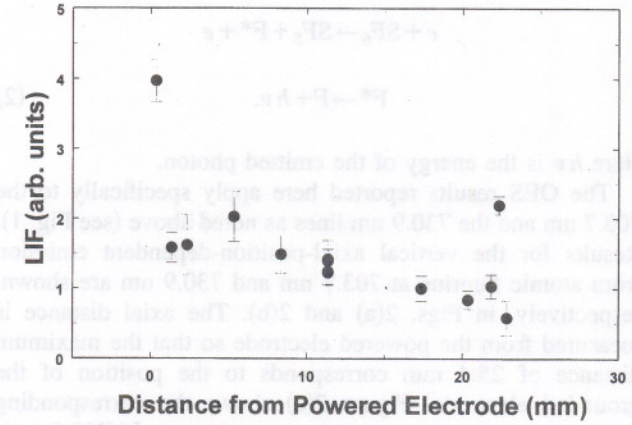

FIG. 3. Axial dependence of the LIF signal at 634.851 nm for a gas pressure of 33.3 Pa and a peak-to-peak applied voltage of 300 V.

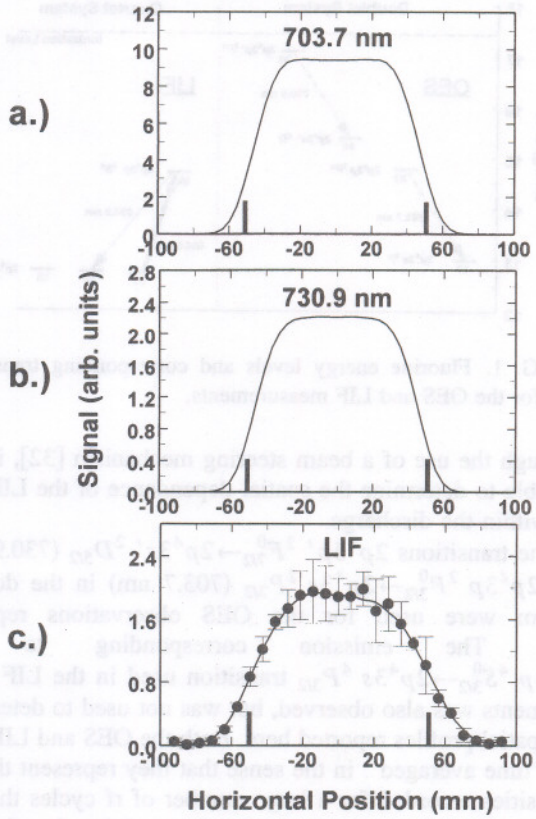

FIG. 4. Horizontal dependence at midgap of the intensities for (a) 703.7 nm emission, (b) 730.9 nm emission, and (c) the 635 nm LIF signal. The OES data have been Abel inverted and all measurements were made for a gas pressure of 33.3 Pa and applied peak-to-peak voltage of 300 V.

spatial dependence. Because of the inherent asymmetry in the geometrical-electrical configuration of the GEC cell [27], the optical emission from the discharge will be vertically asymmetric with respect to the geometrical center of the plasma with a maximum intensity at the powered electrode as seen in Figs. 2 and 3. The narrowness of the sheath near the grounded electrode appears to be consistent with the results discussed below from the IED measurements. The error bars of Fig. 2(c) represent the uncertainty in the ratio measurements based on the standard deviations of the ten current measurements at both wavelengths. The error bars of Fig. 3 represent the standard deviation based on the six different measurements that were taken as mentioned in the preceding section.

The horizontal spatial dependences of the time-averaged OES and LIF intensities at the midpoint between the electrodes are presented in Fig. 4. Figures 4(a), 4(b), and 4(c) show, respectively, the 703.7 nm Abel-inverted results, the 730.9 nm Abel-inverted results, and the LIF data. The horizontal profiles of all three are essentially identical. The intensity distributions are symmetric about the vertical axis as expected from the approximate cyclindrical symmetry of the GEC reference cell.

Figures 5(a) and 5(b) show, respectively, the voltage dependence of the LIF signal for a fixed pressure of 33.3 Pa and the pressure dependence for fixed applied voltages that were adjusted such that $V_1 = 191.6$ V. Both sets of data cor-

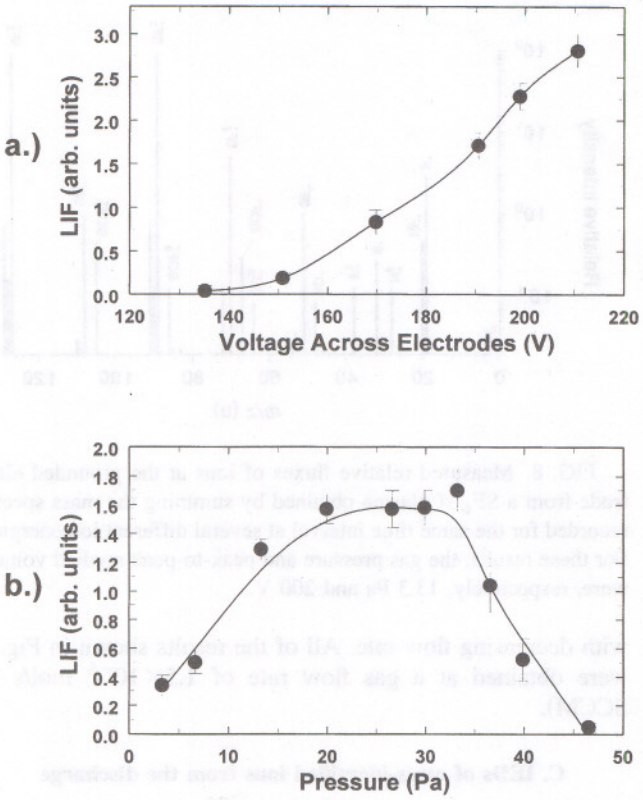

FIG. 5. Dependence of LIF signal at the center of the discharge on (a) voltage V_1 for a fixed pressure of 33.3 Pa; and (b) pressure for a fixed voltage corresponding to $V_1 = 191.6$ V.

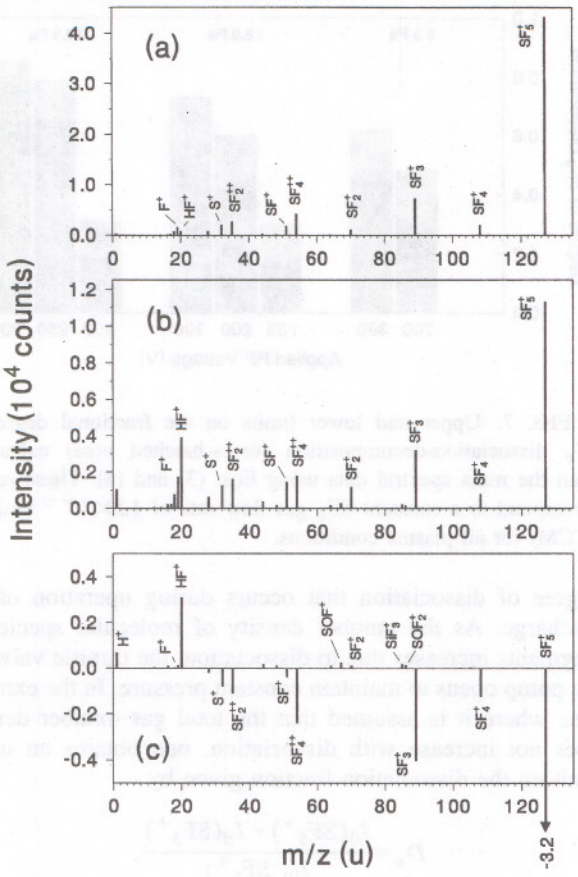

FIG. 6. Mass spectra of neutral species ionized by 70 eV electrons for (a) SF_6 gas sampled from the cell without discharge; (b) gas sampled from the cell with rf discharge (300 V and 33.3 Pa) ignited; and (c) difference of mass spectra (a) and (b) where negative values indicate a loss when the plasma is on. Note the extension of the SF_5^+ line to -3.2. The isotope peaks for sulfur-containing ions have been removed to simplify the spectra.

respond to observations of the 634.9 nm fluorescence at the midpoint along the interelectrode axis. The error bars again represent standard deviations for several repeated measurements. The LIF signal is seen to increase with the voltage V_1 and to go through a maximum as the pressure is increased. The decrease in LIF intensity above 30 Pa is correlated with a decrease in discharge power.

B. Neutral mass spectra and degree of dissociation

Figure 6(a) shows a typical mass spectrum that is observed for SF_6 from the cell when the discharge is off. This spectrum agrees (to within the known uncertainties) with the "standard" SF_6 mass spectrum obtained at a nominal electron-impact energy of 70 eV [37]. The mass spectrum observed when the discharge is turned on is shown in Fig. 6(b). The spectrum recorded in this case exhibits a reduction in the relative intensities of the ions derived from SF_6 such as SF_5^+ and SF_3^+, and the appearance of ions such as HF^+, SOF^+, SOF_2^+, and SiF_3^+ that are associated with discharge-generated decomposition and oxidation products like HF, SF_4, SOF_2, and SiF_4. The species SiF_4 is probably formed from etching of the quartz windows that were mounted on the cell side ports for optical observations. The mass peak at $m/z=32$ u is attributed to S^+, i. e., it does not include a significant contribution from O_2^+, because the ratios of the $m/z=32$ u mass peak to the mass peaks at $m/z=33$ u and $m/z=34$ u are consistent with the known relative abundances for the isotopes of sulfur, and because no significant peak is seen at $m/z=16$ u. The presence of S^+ was also evident in the observed optical-emission spectra for the present experiments, although the signal was weak compared to the F I emission.

The difference mass spectrum obtained by subtracting the mass spectrum recorded when the discharge was on from the mass spectrum recorded for the same length of time and for the same mass-spectrometer settings when the discharge was off is shown in Fig. 6(c). From the difference mass spectrum, it is possible to estimate upper and lower limits on the degree of dissociation-decomposition of SF_6 in the discharge. The estimates were made using the recorded intensities of SF_5^+ for discharge on, $I_{rf}(SF_5^+)$, and for discharge off, $I_0(SF_5^+)$. The SF_5^+ ion was selected because its source is most likely from SF_6 molecules; whereas smaller ions such as SF_3^+ and SF_2^+ could be produced in part from products of SF_6 decomposition.

The unquantified effects of elevated gas pressure due to dissociation and elevated temperature due to discharge heating make it only possible to estimate limits on the dissociation fraction. The pumping system is designed to maintain both a constant gas input flow rate and pressure regardless of whether the discharge is on or off, i.e., independent of the

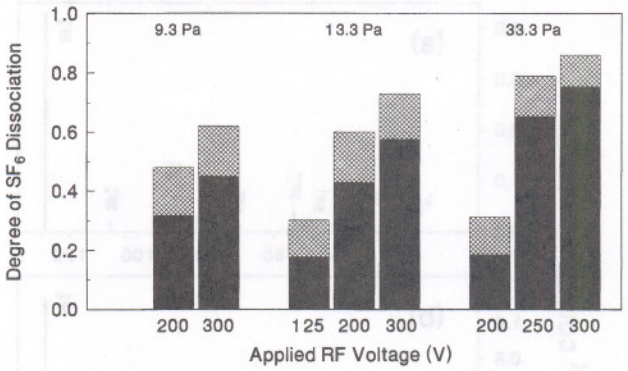

FIG. 7. Upper and lower limits on the fractional degree of SF_6 dissociation-decomposition (cross-hatched area) calculated from the mass spectral data using Eqs. (3) and (4). These results correspond to a constant SF_6 gas flow rate of 1.5×10^{-6} mol/s (2 SCCM) for all plasma conditions.

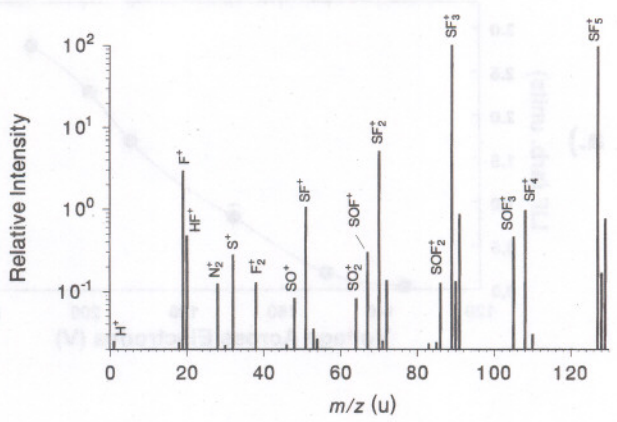

FIG. 8. Measured relative fluxes of ions at the grounded electrode from a SF_6 rf plasma obtained by summing the mass spectra recorded for the same time interval at several different ion energies. For these results, the gas pressure and peak-to-peak applied voltage were, respectively, 13.3 Pa and 200 V.

degree of dissociation that occurs during operation of the discharge. As the number density of molecular species or fragments increases due to dissociation, the throttle valve on the pump opens to maintain constant pressure. In the extreme case where it is assumed that the total gas number density does not increase with dissociation, one obtains an upper limit on the dissociation fraction given by

$$D_u=\frac{I_0(SF_5^+)-I_{rf}(SF_5^+)}{I_0(SF_5^+)}. \tag{3}$$

If, on the other hand, it is assumed that two products are formed from the dissociation of each SF_6 molecule and that the resulting pressure increase is compensated for by the throttling action, one obtains a lower limit for the dissociation fraction given by

$$D_l=\frac{I_0(SF_5^+)-I_{rf}(SF_5^+)}{I_0(SF_5^+)+I_{rf}(SF_5^+)}, \tag{4}$$

which is related to D_u by

$$D_l=\frac{D_u}{2-D_u}. \tag{5}$$

It can be expected that the true value for the dissociation fraction lies between the limits D_u and D_l because some of the dissociation products might recombine [24] through processes such as

$$SF_3+F+M\rightarrow SF_4+M. \tag{6}$$

The degrees of SF_6 dissociation-decomposition in the discharge as calculated from Eqs. (3) and (4) are shown in Fig. 7 for different indicated gas pressures between 9.3 Pa and 33.3 Pa and for different peak-to-peak applied voltages between 125 V and 300 V. The values of D_u and D_l are seen to increase with applied voltage for each pressure, and at the highest voltage and pressure $D_u>0.8$. It is clear from these results that, under some conditions, undissociated SF_6 molecules comprise less than half of the gas in the cell. It is anticipated that the dissociation fraction will also increase with decreasing flow rate. All of the results shown in Fig. 7 were obtained at a gas flow rate of 1.5×10^{-6} mol/s (2 SCCM).

C. IEDs of mass-identified ions from the discharge

Figure 8 shows a mass spectrum (relative fluxes) of ions sampled from the discharge through the orifice in the grounded electrode. The spectrum was constructed by summing mass spectra recorded at several ion energies (from 0.0 eV to the maximum recorded ion energy in 5 eV steps). The gas pressure and applied voltage for this result are, respectively, 13.3 Pa and 200 V. As seen from this figure, the predominant ion under these conditions is SF_3^+ followed by SF_5^+, which agrees with similar observations reported by Nagaseki and co-workers [15]. The triplet structure identified with SF_5^+ and SF_3^+ ions arises from the natural abundances of the different sulfur isotopes (^{32}S, ^{33}S, and ^{34}S). Mass spectra such as are shown in Fig. 8 were found, for a given set of discharge conditions, to be reproducible to within $\pm5\%$ if at least five different ion energies were selected to fall within the main parts of the IEDs shown below (see Fig. 9).

In addition to the main ions (SF_3^+ and SF_5^+) it is seen that there is a measurable contribution to the total flux from other ions derived directly or indirectly from SF_6, namely SF_4^+, SF_2^+, SF^+, and F^+. The ions SOF_3^+, SOF_2^+, SOF^+, SO_2^+, SO^+, and HF^+, which make minor contributions to the total flux, are derived from reactions involving SF_6 oxidation by-products (see, for example, Refs. [3, 24, 38, 39]). Other, larger mass ions, not shown in Fig. 8, such as $S_2F_7^+$, $S_2F_6^+$, and $S_2OF_5^+$ were also observed. Ions that contain two sulfur atoms undoubtedly result from ion-molecule processes, e.g., clustering of ions such as SF^+ with SF_6 molecules, that can occur on surfaces as well as in the gas. These large ions are typically of very low abundance, and the dependence of their abundances on operating parameters such as gas pressure was not systematically investigated. Although the mass filter was adjusted to achieve uniform sensitivity for $m/z\leq127$ u as verified by comparison of

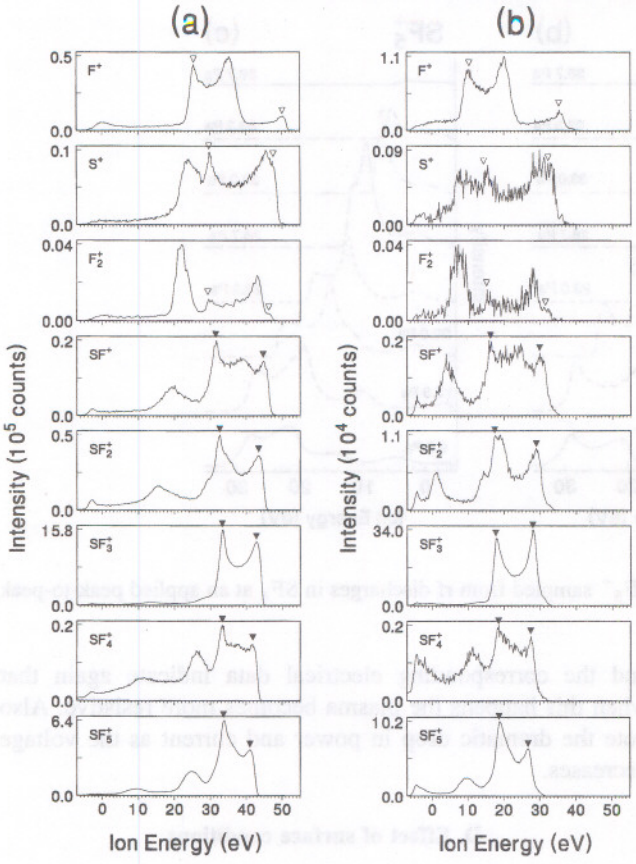

FIG. 9. Measured kinetic-energy distributions for the plasma ions F^+, S^+, F_2^+, SF^+, SF_2^+, SF_3^+, SF_4^+, and SF_5^+ sampled from a SF_6 plasma at a pressure of 13.3 Pa and applied peak-to-peak rf voltage of 200 V. The results in (a) were obtained with a freshly polished grounded electrode, and in (b) with an aged electrode that had been exposed to a SF_6 discharge for several hours. The triangular marks indicate the limits of the saddle structure as discussed in the text.

the neutral mass spectra with reference data [37], we cannot exclude the possibility of mass discrimination at higher masses.

Examples of IEDs measured for selected ions are shown in Figs. 9(a) and 9(b). The data in Fig. 9(a) were obtained after the grounded stainless-steel electrode had been cleaned and polished, and the data in Fig. 9(b) were obtained after the discharge had been operated for many hours during which time a visible coating developed on the grounded electrode surface. The effects of surface conditions on both the optical and IED measurements are discussed in the next section. All data in Fig. 9 were obtained at a gas pressure of 13.3 Pa and applied peak-to-peak rf voltage of 200 V.

The solid triangles in Figs. 9(a) and 9(b) for the relatively high-mass ions ($m/z \geqslant 51$ u) mark the peaks of the "rf-saddle structure" which is characteristic of IEDs from rf discharges under collisionless conditions [40]. The open triangles for the low-mass ions mark the expected extent of the IED saddle width based on the prediction that the width is proportional to $(m/z)^{-1/2}$ and the assumption that the center of the saddle should correspond approximately to the mean (time-averaged) plasma potential [40–43]. A plot of the saddle width versus $(m/z)^{-1/2}$ is shown in Fig. 10. In this

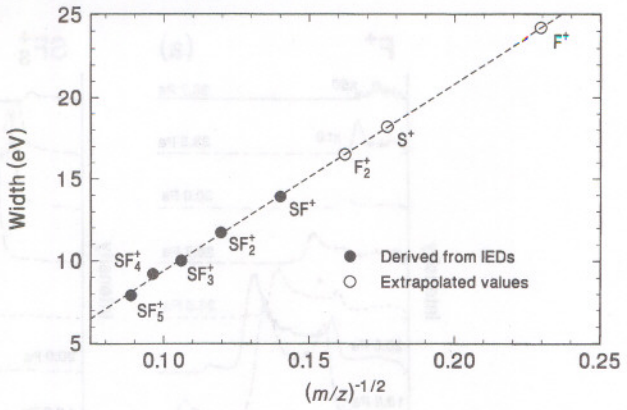

FIG. 10. Energy width of the IED saddle structure versus $(m/z)^{-1/2}$ for the results shown in Fig. 9(b). A linear extrapolation was made using data for heavier ions $m/z \geqslant 51$ u with clearly defined saddles (closed symbols) to determine the saddle widths for the lighter ions for which the complexity of the distributions causes ambiguities in defining the saddle limits (open symbols).

figure, the open points for low-mass ions correspond to an extrapolation from the results for the high-mass ions that are plotted using closed symbols. The results shown in Fig. 10 correspond to the coated electrode case given in Fig. 9(b). However, the saddle widths differ only slightly from those observed using a freshly polished electrode (see Fig. 9).

The saddle structure is most clearly defined for the predominant ion SF_3^+. In the case of the lower-mass ions, the rf-saddle structure is not so well defined, and secondary peaks appear within the limits of the saddle. Secondary peaks also appear in some cases at energies below the saddle that probably result from energy losses due to ion-molecule collisions within the plasma sheath [33,34,42]. Possible explanations for the secondary peaks that appear within the saddle limits will be considered later. The mass-dependent features that are characteristic of the measured IEDs are relatively independent of the electrode condition as can be seen from comparing the results shown in Figs. 9(a) and 9(b).

Figures 11(a), 11(b), and 11(c) show the pressure dependence of the IEDs, respectively, for the ions F^+, SF_3^+, and SF_5^+ sampled from rf discharges in SF_6 at a constant applied peak-to-peak voltage of 200 V. The corresponding pressure dependences of the measured electrical parameters are shown in Fig. 12. The data presented in both Figs. 11 and 12 were obtained under coated electrode conditions, i.e., after the discharge had been operated for several hours. Similar results were obtained using freshly polished electrodes, for all electrical parameters except V_b, which will be discussed later.

It is seen that as pressure increases the saddle structure becomes increasingly more constricted and the mean energy of the saddle, corresponding to the mean plasma potential, shifts to lower values (from about 25.5 eV at 9.3 Pa to about 2.0 eV at 36.7 Pa). However, the general features characteristic of the saddle structure for each ion appear to be preserved as pressure decreases. The observed pressure dependence of the IEDs appears to be consistent with a constriction in the size of the sheath and with a corresponding decrease in the mean plasma potential (and thus a smaller voltage drop across the sheath in front of the grounded elec-

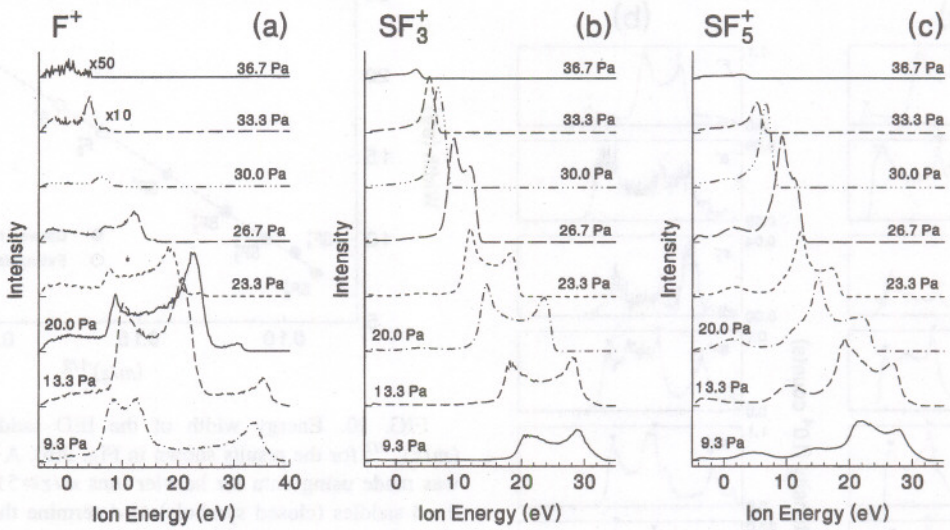

FIG. 11. Pressure dependence of IEDs for (a) F^+, (b) SF_3^+, and (c) SF_5^+ sampled from rf discharges in SF_6 at an applied peak-to-peak voltage of 200 V.

trode) as pressure is increased. The constriction in the sheath is also reflected in the data on the electrical parameters that show a decrease in ϕ_1 with pressure and a corresponding increase in the plasma impedance that are indicative of a plasma that is becoming more "resistive" in the bulk with increasing pressure, i.e., the voltage drop across the bulk becomes dominant. This behavior is also consistent with previous observations and predictions [7,8,21] about rf plasmas in SF_6.

A similar change in the IED characteristics occurs when the pressure is kept constant and the applied voltage is changed as shown by the results for SF_3^+ presented in Fig. 13. The corresponding changes in the electrical parameters for this case are given in Fig. 14. The results shown in Figs. 13 and 14 were obtained under coated electrode conditions and for a gas pressure 13.3 Pa. As the applied voltage is decreased at this pressure, the size of the sheath decreases and the corresponding electrical data indicate again that when this happens the plasma becomes more resistive. Also note the dramatic drop in power and current as the voltage decreases.

D. Effect of surface conditions

As suggested by the results presented in the preceding section, operation of a rf discharge in SF_6 can alter surfaces, especially the electrode surfaces, within the cell. The nature of this surface alteration is not known, but obviously has a significant effect on the observed characteristics of the discharge. Apparent downward shifts of about 11 eV in the maximum and mean ion energies are evident from a comparison of the IED data in Figs. 9(a) and 9(b) in going from a freshly polished to a coated electrode. The downward shift in ion energies also corresponds to an observed decrease in

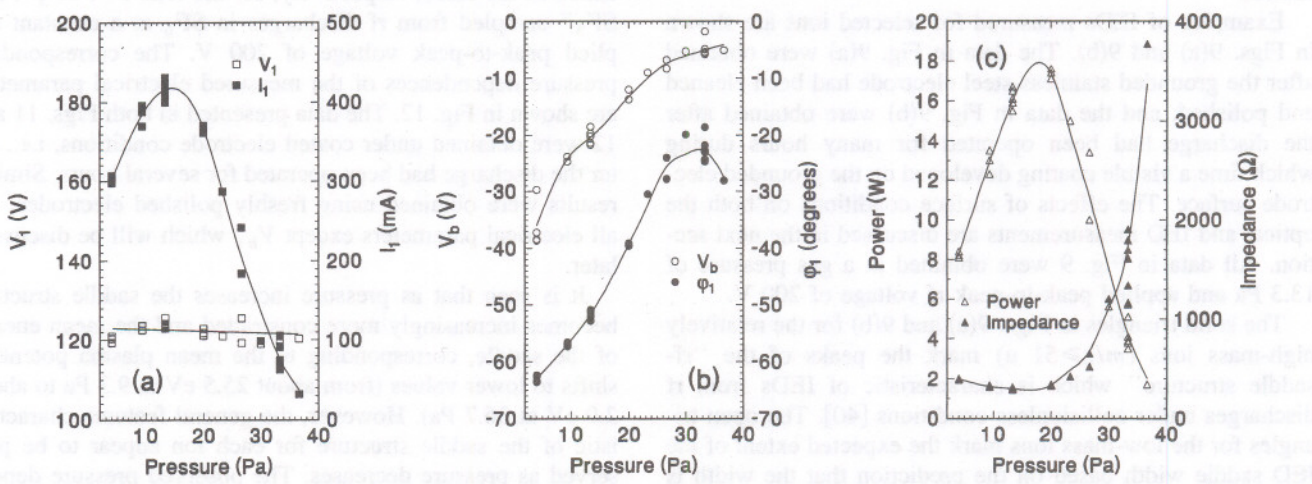

FIG. 12. Measured pressure dependence of the electrical parameters for SF_6 discharges corresponding to results shown in Fig. 11. Shown are (a) the voltage and current Fourier amplitudes at the fundamental frequency (V_1 and I_1); (b) the self-bias voltage V_b and phase difference (ϕ_1) between V_1 and I_1; and (c) the power dissipated in the discharge and the plasma impedance.

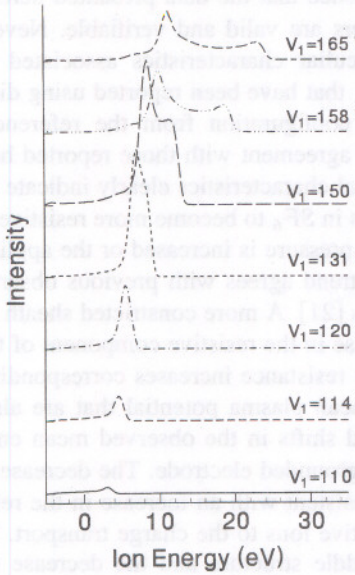

FIG. 13. Voltage dependence of the IEDs for SF_3^+ sampled from rf discharges in SF_6 at a gas pressure of 13.3 Pa.

the absolute magnitude of the bias potential V_b of about the same magnitude. After continuous exposure to the discharge for several hours, the surface of the grounded stainless-steel electrode was observed to acquire a bluish hue which is possibly associated with deposition of a dielectric, perhaps polymeric, coating of much lower conductivity than the original metallic surface.

The possible effects that an insulating or partially insulating coating on the electrode surface can have on the discharge and recorded distribution in energy of ions that hit the electrode surface was the subject of a recent investigation using the GEC reference cell [34,44]. It was argued that the presence of a quasipermanent, stationary charge distribution can shift the potential of the electrode surface relative to the local ground potential which serves as a reference point in the recording of ion energies. This can give rise to an apparent downward shift in *recorded* ion energy which, under some conditions, results in the assignment of "negative" values to the energy. If this happens, the recorded ion energy will not be a true measure of the kinetic energy that the ion actually possesses when it strikes the electrode surface [45].

In some cases, as observed previously for rf discharges in oxygen [44], the plasma potential may remain constant with respect to the electrode surface and therefore shift relative to the local ground potential. In this event, the shift in recorded ion energies may simply reflect the adjustment in the plasma potential relative to ground. However, in the case of SF_6, there is evidence from independent LIF (Fig. 15) and corresponding electrical measurements (Fig. 16) that the discharge characteristics also change significantly in response to electrode aging. Hence, in this case, the plasma potential may change with respect to the electrode surface as the surface coating changes. The LIF data in Fig. 15 were obtained from observations made at the geometrical center of the interelectrode gap at a gas pressure of 33.3 Pa and an applied peak-to-peak voltage of 300 V. These data were recorded for a 350 min time interval immediately after the surfaces in the cell had been cleaned by exposure to a continuous, prolonged rf discharge in argon. The argon discharge is evidently effective in removing material from the electrode surfaces by the process of ion sputtering [44]. The vertical error bars represent standard deviations from results of several repeated measurements and the horizontal error bars indicate the uncertainties due to the extent of the finite time interval for the measurements. It is seen that during electrode aging the LIF intensity at 624 nm decreases significantly. The corresponding data on the electrical parameters shown in Fig. 16 indicate very rapid initial changes in the discharge characteristics especially within the first few minutes of discharge operation. This rapid change might explain the negative recorded energies seen in Fig. 9 even for the case of a polished electrode. From the data on ϕ_1 and impedance, the

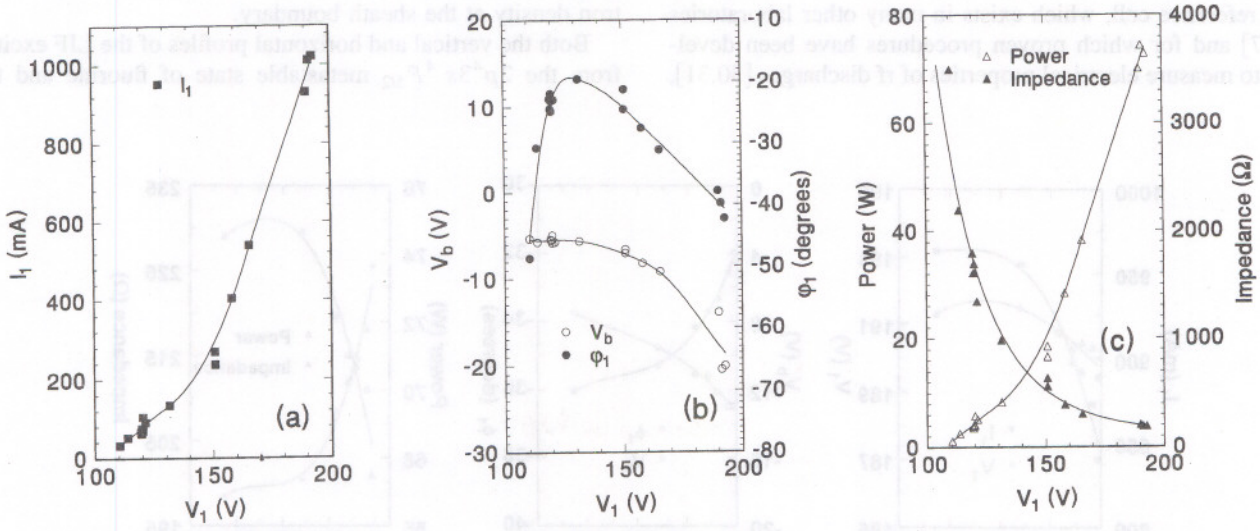

FIG. 14. Measured dependence of electrical parameters for SF_6 discharges corresponding to the IED data shown in Fig. 13. Shown are (a) the amplitude for the fundamental Fourier component of the current (I_1); (b) the self-bias voltage V_b and phase difference (ϕ_1) between V_1 and I_1, and (c) the power dissipated in the plasma and the plasma impedance.

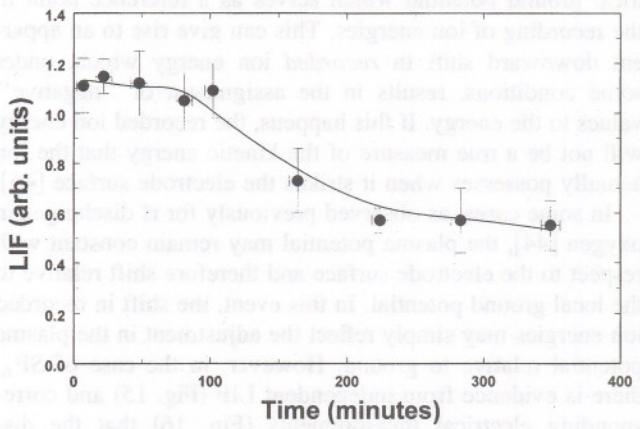

FIG. 15. Dependence of the LIF signal on time after starting with electrodes that were "cleaned" in an argon plasma. The data were taken at a gas pressure of 33.3 Pa and applied peak-to-peak voltage of 300 V.

discharge appears to become more capacitive with time, i.e., less resistive. The discharge current and power dissipation also show increases with time, and the LIF intensity appears in this case to be inversely correlated with the power dissipation.

IV. DISCUSSION AND CONCLUSIONS

The results presented here from LIF, OES, neutral mass spectrometry, IED measurements, and corresponding electrical measurements provide a more comprehensive and consistent characterization of 13.56 MHz rf discharges in SF_6 than has been possible from previous experiments. It is anticipated that the present results should prove useful both in the validation of theoretical models for SF_6 discharges and in the interpretation of previously obtained experimental results. Because the investigation was performed using the GEC reference cell, which exists in many other laboratories [26,27] and for which proven procedures have been developed to measure electrical properties of rf discharges [30,31], one has confidence that the data presented here on the electrical parameters are valid and verifiable. Nevertheless, the trends and peculiar characteristics associated with rf discharges in SF_6 that have been reported using discharge cells that differ in configuration from the reference cell were found to be in agreement with those reported here.

The electrical characteristics clearly indicate the tendency of rf discharges in SF_6 to become more resistive than capacitive as the gas pressure is increased or the applied voltage is reduced. This trend agrees with previous observations [7,8] and predictions [21]. A more constricted sheath is associated with the increase in the resistive component of the discharge impedance. As resistance increases corresponding decreases occur in the mean plasma potential that are also correlated with downward shifts in the observed mean energy of ions that strike the grounded electrode. The decrease in $|V_b|$ with pressure is consistent with an increase in the relative contribution of negative ions to the charge transport. The collapse of the IED saddle structure and the decrease of mean ion energies reported here for increasing gas pressures also agrees with earlier experimental results obtained by Thompson and co-workers [17] using retarding potential analysis. However, it is clear that the interpretation of the IED structure in SF_6 discharges obtained by this method is confounded by relative contributions from the ions of different mass observed here.

The OES and LIF spatial intensity distribution profiles exhibit sharp maxima in narrow regions in front of the electrode surfaces that are also consistent with a constricted sheath. The vertical OES and LIF intensity profiles exhibit secondary maxima suggestive of the double-layer formation in the sheath predicted by Tsai and Wu [20] and Nakano and co-workers [21] and observed by Petrović and co-workers [10] in spatiotemporal profiles of nitrogen emission from rf discharges in SF_6-N_2 mixtures that contain 10% N_2 (also see Ref. [42]). The observed maxima in the vertical OES profiles are also consistent with the model predictions of Gogolides and co-workers [11] and Govindan and Meyyappan [22] which indicate enhancements in time-averaged electron density at the sheath boundary.

Both the vertical and horizontal profiles of the LIF excited from the $2p^4 3s\ ^4P_{5/2}$ metastable state of fluorine and the

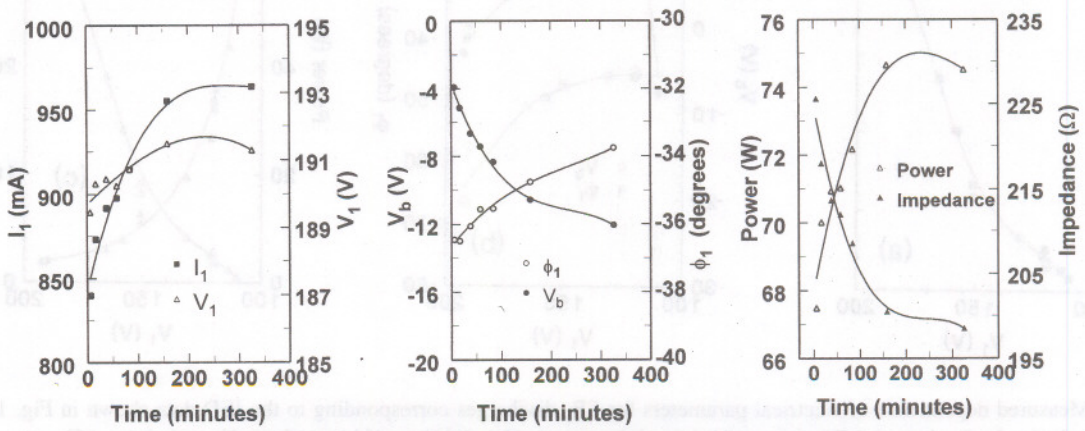

FIG. 16. Time dependence of measured electrical parameters corresponding to the LIF results shown in Fig. 15.

emissions from the $2p^4 3p'\ ^2F^0_{7/2}$ and $2p^4 3p\ ^2P_{3/2}$ excited states of fluorine have the same general shapes as expected. The enhancement in the emission intensity ratio, $I(730.9\text{nm})/I(703.7\text{nm})$, in the sheath boundary regions in front of the electrodes is consistent with a higher mean electron energy in these regions and correlates well with the predicted corresponding enhancements in ionization rate as given in the work of Paranjpe and co-workers [19], Nakano and co-workers [21], and Govindan and Meyyappan [22].

The observed relative contributions to the total ion flux from ions of different mass are undoubtedly influenced by ion-molecule processes in the discharge such as

$$SF_4^+ + SF_6 \rightarrow SF_5 + SF_5^+ \quad (7)$$

invoked by de Urquijo-Carmona and co-workers [46] to account for the relatively low intensities of SF_4^+ observed in drift-tube and corona-discharge experiments [38]. The results from the present work also indicate that in low-pressure rf discharges, SF_4^+ makes only a minor contribution to the total ion flux that impinges on the grounded electrode. The predominance of SF_3^+ and SF_5^+ reported here agrees with the recent results of Nagaseki and co-workers [15].

Important processes that can affect the relative contributions of SF_3^+ and SF_5^+ to the total ion flux and lead to formation of ions such as $S_2F_7^+$ observed here have been investigated by Talib and Saporoschenko [47] and include

$$SF_5^+ + SF_6 \rightarrow SF_3^+ + SF_6 + F_2 \quad (8)$$

and

$$SF_3^+ + SF_6 \rightarrow S_2F_9^{+*} \rightarrow S_2F_7^+ + F_2. \quad (9)$$

Process (8), which has a rate at low energies that is more than an order of magnitude greater than that of process (9), could be responsible for the conversion of SF_5^+ (the predominant ion produced from SF_6 by electron impact [48]) into SF_3^+, the predominant ion observed here under most rf-discharge conditions.

Any model used to interpret the data on relative ion fluxes must necessarily take into account the fact, as reported here, that a significant fraction of the SF_6 in the discharge is either dissociated or decomposed to form lower valence sulfur fluorides or oxyfluorides such as SF_2, SF_4, and SOF_2. This is especially true for the relatively low gas flow rates used in the present experiments where the degree of SF_6 dissociation was found from neutral mass spectrometry to approach 80% at the highest pressures and applied voltages. In present models of rf discharges in SF_6 [17–22], it is generally assumed that SF_6 is the predominant neutral species responsible for such processes as ionization, electron attachment, detachment, and momentum transfer. Inasmuch as the models neglect processes involving neutral dissociation or decomposition products, they are incorrect and may have a limited range of applicability. The fact that the models which neglect dissociation products still yield, for example, predictions of the electrical characteristics that qualitatively agree with the experimental results reported here may be partly a consequence of the fact that the products of SF_6 dissociation are also predominantly highly electronegative [49]. This is based on the assumption that the mere presence of high negative-ion concentrations has a dominant effect on the electrical properties.

The basis for the deviations from simple rf-saddle structure that appears in the measured IEDs of some lighter ions in the SF_6 discharge remains a mystery and a challenge to future theoretical work. The results from the present measurements show, in fact, that the peaks attributed to the rf saddle are often minor features in the case of the lighter ions, even though they are the most prominent peaks in the case of the heavier ions for the same plasma conditions.

In a recent work by Vender and co-workers [50], it was shown that the IEDs of light minority ions sampled at the electrode surfaces can contain secondary features in the saddle structure that result from ion bunching which is related to the Bohm and sheath velocities. It is not clear, however, that this effect can account for the relatively large intermediate features seen, for example, in the distributions for F^+ reported here.

The structure of the IEDs for the lighter ions from SF_6 discharges may also be due, in part, to the effects of the double-layer formation which is characteristic of the sheath in these discharges. Moreover, because of the relatively large widths of the rf saddles for some of these ions, one must be concerned about possible interference from low-energy features associated with collisional energy degradation in the sheath that can appear within the saddle [51]. As seen in Fig. 9, these secondary features can themselves exhibit saddle structures which may superimpose on the main rf saddle. Peaks occur at energies below the saddle that may be attributed to the effect of collisions in the sheath.

Finally, attention should be drawn to the significant problem of surface conditioning by a SF_6 discharge that is evident from results of electrical, optical, and ion measurements reported here. It is speculated that these effects are associated with formation of insulating, or partially insulating deposits on the electrode surfaces. Evidence of significant surface fluorination has been reported in previous investigations of rf discharges in SF_6 at low pressures [1,39,52]. Stationary static charge that occurs on electrode surfaces that become partially insulating can influence the electrical properties of the discharge and cause shifts in recorded ion energies that are then susceptible to misinterpretation [44]. At present, rf-discharge models do not treat cases where electrode surfaces become insulating and can retain charge. The results presented here and in our earlier work [44] clearly show that surface effects are important and it may not be correct to assume that the electrodes are perfect metallic equipotential surfaces, especially after the discharge has been in operation for some time.

ACKNOWLEDGMENTS

The authors are grateful for the interest in this work shown by M. Schmidt of INP and L. G. Christophorou of NIST, and for the assistance provided by T. Weber from Bryn Mawr College. The work was performed at NIST. R. Foest was supported by NIST and by the German Academic Exchange Service (DAAD).

[1] G. Turban, J. F. Coulon, and N. Mutsukura, Thin Solid Films **176**, 289 (1989).
[2] A. Picard, G. Turban, and B. Grolleau, J. Phys. D **19**, 991 (1986).
[3] A. Picard and G. Turban, Plasma Chem. Plasma Proc. **5**, 333 (1985).
[4] K. M. Eisele, J. Electrochem. Soc. **128**, 123 (1981).
[5] J. Jorné, K. C. Cadien, and J. E. Shoenholtz, J. Electrochem. Soc. **137**, 3683 (1989).
[6] R. d'Agostino and D. L. Flamm, J. Appl. Phys. **52**, 162 (1981).
[7] H. Shan, Ph.D. thesis, Stanford University, 1991.
[8] S. Kakuta, Z. Lj. Petrović, F. Tochikubo, and T. Makabe, J. Appl. Phys. **74**, 4923 (1993).
[9] S. B. Radovanov, B. Tomcik, Z. Lj. Petrović, and B. M. Jelenković, J. Appl. Phys. **67**, 97 (1990).
[10] Z. Lj. Petrović, F. Tochikubo, S. Kakuta, and T. Makabe, J. Appl. Phys. **73**, 2163 (1993).
[11] E. Gogolides, J-P. Nicolai, and H. H. Sawin, J. Vac. Sci. Technol. A **7**, 1001 (1989).
[12] S. Suganomata, I. Ishikawa, J. Tanaka, and H. Ozaki, Jpn. J. Appl. Phys. **30**, 180 (1991).
[13] A. Utagikar and B. E. Thompson, J. Vac. Sci. Technol. A **10**, 1201 (1992).
[14] A. Kono, M. Endo, K. Ohata, S. Kishimoto, and T. Goto, J. Appl. Phys. **76**, 7221 (1994).
[15] K. Nagaseki, H. Kobayashi, I. Ishikawa, E. Nishimura, Y. Saito, and S. Suganomata, Jpn. J. Appl. Phys. **33**, 4348 (1994).
[16] I. Ishikawa, K. Nagaseki, H. Kusunoki, E. Nishimura, Y. Saito, and S. Suganomata (unpublished).
[17] B. E. Thompson, K. D. Allen, A. D. Richards, and H. H. Sawin, J. Appl. Phys. **59**, 1890 (1986).
[18] L. E. Kline, IEEE Trans. Plasma Sci. **PS-14**, 145 (1986).
[19] A. P. Paranjpe, J. P. McVittie, and S. A. Self, Phys. Rev. A **41**, 6949 (1990).
[20] J. H. Tsai and C. Wu, Phys. Rev. A **41**, 5626 (1990).
[21] N. Nakano, N. Shimura, Z. Lj. Petrović, and T. Makabe, Phys. Rev. E **49**, 4455 (1994).
[22] T. R. Govindan and M. Meyyappan, U.S. Dept. of Commerce Report No. 50-DKNA-3-00143, 1995 (unpublished); M. Meyyappan and T. R. Govindan, Bull. Am. Phys. Soc. **40**, 15 667 (1995).
[23] R. Morrow, IEEE Trans. Plasma Sci. **PS-14**, 234 (1986).
[24] R. J. Van Brunt and J. T. Herron, IEEE Trans. Electr. Insul. **25**, 75 (1990); Phys. Scr. **T53**, 9 (1994).
[25] D. B. Ogle and G. A. Woolsey, J. Phys. D **20**, 453 (1987).
[26] J. K. Olthoff and K. E. Greenberg, J. Res. Natl. Inst. Stand. Technol. **100**, 327 (1995).
[27] P. J. Hargis, K. E. Greenberg, P. A. Miller, J. B. Gerardo, J. R. Torczynski, M. E. Riley, G. A. Hebner, J. R. Roberts, J. K. Olthoff, J. R. Whetstone, R. J. Van Brunt, M. A. Sobolewski, H. A. Anderson, M. P. Splichal, J. L. Mock, P. Bletzinger, A. Garscadden, R. A. Gottscho, G. Selwyn, M. Dalvie, J. E. Heidenreich, J. W. Butterbaugh, M. L. Brake, M. L. Passow, J. Pender, A. Lujan, M. E. Elta, D. B. Graves, H. H. Sawin, M. J. Kushner, J. T. Verdeyen, R. Horwath, and T. R. Turner, Rev. Sci. Instrum. **65**, 140 (1994).
[28] E. Benck, T. Weber, and J. Roberts, Bull. Am. Phys. Soc. **40**, 1555 (1995).
[29] R. Foest, J. K. Olthoff, and R. J. Van Brunt, Bull. Am. Phys. Soc. **40**, 1572 (1995).
[30] M. A. Sobolewski, J. Res. Natl. Inst. Stand. Technol. **100**, 341 (1995).
[31] M. A. Sobolewski, J. Vac. Sci. Technol. A **10**, 3350 (1992).
[32] J. R. Roberts, J. Res. Natl. Inst. Stand. Technol. **100**, 353 (1995).
[33] J. K. Olthoff, R. J. Van Brunt, S. B. Radovanov, J. A. Rees, and R. Surowiec, J. Appl. Phys. **75**, 115 (1994).
[34] J. K. Olthoff, R. J. Van Brunt, and S. B. Radovanov, J. Res. Natl. Inst. Stand. Technol. **100**, 383 (1995).
[35] J. L. Forand, K. Becker, and J. W. McConkey, Can. J. Phys. **64**, 269 (1986).
[36] K. A. Banks, A. E. Tabor, and K. Becker, J. Chem. Phys. **86**, 4871 (1987).
[37] A. Cornu and R. Massot, *Compilation of Mass Spectral Data*, 2nd ed. (Heyden, New York, 1975), Vol. 1, p. 77A; *Eight Peak Index of Mass Spectra* (AWRE, Aldermaston, 1974), Vol. 1, p. 153.
[38] I. Sauers and G. Harman, J. Phys. D **25**, 774 (1992).
[39] R. J. M. M. Snijkers, J. F. Coulon, and G. Turban, J. Phys. D **24**, 1098 (1991).
[40] R. T. C. Tsui, Phys. Rev. **168**, 107 (1968).
[41] P. Benoit-Cattin and L.-C. Bernard, J. Appl. Phys. **169**, 5723 (1968).
[42] D. Field, D. F. Klemperer, P. W. May, and Y. P. Song, J. Appl. Phys. **70**, 82 (1992).
[43] R. J. M. M. Snijkers, M. J. M. van Sambeek, G. M. W. Kroesen, and F. J. deHoog, Appl. Phys. Lett. **63**, 308 (1993).
[44] J. K. Olthoff, R. J. Van Brunt, and S. B. Radovanov, Appl. Phys. Lett. **67**, 473 (1995).
[45] T. Makabe, F. Tochikubo, and M. Nishimura, Phys. Rev. A **42**, 3674 (1990).
[46] J. de Urquijo-Carmona, C. Cisneros, H. Martinez, and I. Alvarez, J. Phys. D **25**, 1277 (1992).
[47] Z. A. Talib and M. Saporoschenko, Int. J. Mass Spectrom. Ion Phys. **116**, 1 (1992).
[48] V. H. Dibeler and F. L. Mohler, J. Res. Natl. Bur. Stand. **40**, 25 (1948).
[49] H.-X. Wan, J. H. Moore, J. K. Olthoff, and R. J. Van Brunt, Plasma Chem. Plasma Proc. **13**, 1 (1993).
[50] D. Vender, G. M. W. Kroesen, and F. J. de Hoog, Phys. Rev. E **51**, 3480 (1995).
[51] S. Biehler, thesis, University of Bochum, 1991.
[52] Y. Khairallah, F. Khonsari-Arefi, and J. Amouroux, Pure Appl. Chem. **66**, 1353 (1994).